HHS Public Access

Author manuscript

Int J Cardiol. Author manuscript; available in PMC 2019 December 15.

Published in final edited form as:

Int J Cardiol. 2018 December 15; 273: 168–176. doi:10.1016/j.ijcard.2018.09.073.

Sarcomere-based genetic enhancement of systolic cardiac function in a murine model of dilated cardiomyopathy

Jiayang Li[a,1], **Kenneth S. Gresham**[b,1], **Ranganath Mamidi**[a,1], **Chang Yoon Doh**[a,1], **Xiaoping Wan**[c,1], **Isabelle Deschenes**[a,c,1], and **Julian E. Stelzer**[a,*,1]

[a]Department of Physiology and Biophysics, School of Medicine, Case Western Reserve University, Cleveland, OH, United States of America

[b]Center for Translational Medicine, Lewis Katz School of Medicine, Temple University, Philadelphia, PA, United States of America

[c]The Heart and Vascular Research Center, Metro Health, Cleveland, OH, United States of America

Abstract

Diminished cardiac contractile function is a characteristic feature of dilated cardiomyopathy (DCM) and many other heart failure (HF) causing etiologies. We tested the hypothesis that targeting the sarcomere to increase cardiac contractility can effectively prevent the DCM phenotype in muscle-LIM protein knockout ($MLP^{-/-}$) mice. The ablation of cardiac myosin binding protein C ($MYBPC3^{-/-}$) protected the $MLP^{-/-}$ mice from developing the DCM phenotype. We examined the in vivo cardiac function and morphology of the resultant mouse model lacking both MLP and MYBPC3 (DKO) by echocardiography and pressure-volume catheterization and found a significant reduction in hypertrophy, as evidenced by normalized wall thickness and chamber dimensions, and improved systolic function, as evidenced by enhanced ejection fraction (~26% increase compared $MLP^{-/-}$ mice) and rate of pressure development (DKO 7851.0 ± 504.8 vs. $MLP^{-/-}$ 4496.4 ± 196.8 mmHg/s). To investigate the molecular basis for the improved DKO phenotype we performed mechanical experiments in skinned myocardium isolated from WT and the individual KO mice. Skinned myocardium isolated from DKO mice displayed increased Ca^{2+} sensitivity of force generation, and significantly accelerated rate of cross-bridge detachment (+63% compared to $MLP^{-/-}$) and rate of XB recruitment (+58% compared to $MLP^{-/-}$) at submaximal Ca^{2+} activations. The in vivo and in vitro functional enhancement of DKO mice demonstrates that enhancing the sarcomeric contractility can be cardioprotective in HF characterized by reduced cardiac output, such as in cases of DCM.

---

[1]This author takes responsibility for all aspects of the reliability and freedom from bias of the data presented and their discussed interpretation.

[*]Corresponding author at: 2109 Adelbert Rd, Robbins E522, Department of Physiology and Biophysics, School of Medicine, Case Western Reserve University, Cleveland, OH 44106, United States of America. julian.stelzer@case.edu (J.E. Stelzer).

Competing interests

The authors report no relationships that could be construed as a conflict of interest.

Appendix A. Supplementary data

Supplementary data to this article can be found online at https://doi.org/10.1016/j.ijcard.2018.09.073.

Keywords

Dilated cardiomyopathy; Contractility; Heart failure

1. Introduction

Heart failure (HF) is a leading cause of morbidity and mortality, affecting approximately 40 million people worldwide [1]. HF is characterized by chronic cardiac insufficiency and is an end stage syndrome that can result from a multitude of conditions such as cardiomyopathies (CMs), disorders that arise due to intrinsic defects or direct damage of the myocardial contractile machinery. The two most common forms of CMs are dilated cardiomyopathy (DCM) and hypertrophic cardiomyopathy (HCM). Whereas DCM is defined by poor systolic function with eccentric hypertrophy and ventricular chamber dilation, HCM is characterized by concentric hypertrophy and reduced ventricular chamber size that impairs filling and diastolic function.

Although understanding the molecular etiologies of DCM and HCM have been greatly aided by advancements in genome sequencing, the identification of causative genes in CMs have not yet translated to significant advancements in treatment. This is mainly due to gaps in knowledge of how primary genetic defects trigger nonspecific secondary physiologic and or pathologic remodeling. The number of identified CM-related gene mutations are currently over a thousand and continues to increase, involving N50 genes [2]. Further highlighting the complex pathogenesis of DCM is the list of gene mutations that encode proteins involved in force generation and transduction, Ca^{2+} handling, and mitochondrial energy production [1]. Furthermore, some of the newly identified DCM mutations are often rare or private variants found in only a single family [1], thus limiting positive identification and characterization of whether the variants are truly pathogenic, susceptibility modifying, or benign. Therefore, insights that can unify the diversity of genotypes' influence on DCM phenotype will be important in guiding clinical management and designing novel therapies.

Differences in cardiac myofilament contractility are also dependent on the etiology of DCM, mutations could result in decreased force generation or impaired Ca^{2+} homeostasis [3,4]. In a murine model of DCM, muscle LIM-protein (MLP) ablation induced ventricular dilation and contractile dysfunction that closely resembles the human DCM phenotype [5]. The clinical relevance of MLP, also known as CSRP3, is highlighted by a growing body of evidence that have identified a number of DCM and HCM associated mutations [6–8]. Studies have since identified that MLP localizes to the Z-disc, costameres, and intercalated discs, where it is believed to aid in force conduction between the sarco-mere and sarcolemma [9,10]. While the relationship between hypocontractile $MLP^{-/-}$ cardiomyocytes and pathologic DCM remodeling remains poorly understood, it is possible to test if normalizing power output in $MLP^{-/-}$ hearts can improve overall function. Results from previous studies have led to a common view that DCM mutations cause hypocontractility and HCM mutations cause hypercontractility [11–15]. Thus, to assess the feasibility of normalizing power output in $MLP^{-/-}$ myocardium, we increased force generation at the

sarcomere level by using a hypercontractile HCM model lacking MYBPC3, which encodes cardiac myosin-binding protein C (cMyBPC).

In this context, recent efforts to improve cardiomyocyte contractility have focused on targeting the force generating machinery within the sarcomere [16–19]. Unlike currently available HF therapies that focus on blocking upstream neurohormonal pathways (RAAS inhibitors, β-adrenergic blockers, and aldosterone antagonists) which do not directly improve cardiac contractile function [20], sarcomere-directed therapy promotes actomyosin cross-bridge (XB) interactions which dictate the rate and magnitude of force generation in cardiac muscle. For example, we recently showed that the selective cardiac myosin activator, omecamtiv mecarbil (OM), prolongs XB force generation and enhances XB recruitment and that the effects of OM are influenced by the presence of cMyBPC [21].

Within the cardiac sarcomere, cMyBPC is an important regulator of actomyosin XB interactions. Previous studies have shown that cMyBPC phosphorylation or ablation relieves physical constraints on actomyosin interactions and cause significant acceleration of XB cycling kinetics, thus increasing both XB recruitment and detachment rates [22–24]. At the whole heart level, the hypercontractile MYBPC3$^{-/-}$ hearts exhibited significant concentric hypertrophy and impaired diastolic and systolic function [25]. Thus, we hypothesized that superimposing the MYBPC3$^{-/-}$ hypercontractile phenotype onto the MLP$^{-/-}$ hypocontractile DCM phenotype will normalize power output and thereby protect the heart from pathogenic stress. To test our hypothesis, we generated a novel MLP/MYBPC3 double knockout (DKO) transgenic (TG) mouse and studied both in vivo whole heart function and in vitro XB behavior.

2. Methods

2.1. Transgenic animals

MLP$^{-/-}$ mice [5] and MYBPC3$^{-/-}$ mice [25], both of 129SV background, were generated previously. DKO mice were generated by breeding homozygous male and female MLP$^{-/-}$ mice with homozygous male and female MYBPC3$^{-/-}$ mice. Expected Mendelian ratios of DKO offspring were obtained, indicating no embryonic lethality. DKO mice were viable, appeared normal in all respects, and had a normal lifespan. Early postnatal pheno-type reported in the MLP$^{-/-}$ mice [5] were not observed in the DKO mice. All procedures involving animal care and handling were reviewed and approved by the Case Western Reserve University Animal Care and Use Committee.

2.2. Histological analysis of cardiac tissue

Hearts were fixed with 4% paraformaldehyde, embedded in paraffin for 5 μm serial sectioning, and staining as previously described [26]. Quantitative analysis of trichrome stained sections were performed using ImageJ (National Institutes of Health, USA) that measured number of pixels where the blue intensity exceeded the red intensity by N120% [27].

2.3. Western blot and pro-Q analysis of myocardial samples

Myocardial and membrane associated proteins were studied as previously described [26]. Briefly, frozen LV tissue was homogenized and solubilized in reducing Laemmli buffer. Proteins were separated using SDS-PAGE electrophoresis. Westerns were transferred to PVDF membranes and incubated overnight at 4 °C with primary antibodies. Densitometric scanning of Western blots and stained gels was performed using Image J software (U.S. National Institutes of Health).

2.4. Immunohistochemistry (IHC) staining

IHC fluorescent staining of α-actinin was performed on skinned myocardium isolated from hearts of each experimental group (refer to the supplemental methods for the detailed protocol).

2.5. In vivo cardiac function

Noninvasive transthoracic echocardiography and pressure-volume loop analysis was performed on anesthetized (1.5–2% isoflurane) 10 (±0.5) week old mice as previously described [28], Pressure-volume (P-V) loop analysis was performed on anesthetized and ventilated (1.5–2% isoflurane) mice as previously described [28].

2.6. Experimental protocols in skinned myocardium experiments

Steady-state and cross-bridge kinetic measurements in skinned ventricular were performed as described previously [26,29]. Briefly, multicellular preparations were permeabilized with 1% TritonX100 for 1 h. Calcium activated force was measured at sarcomere length of 2.1 μm. The force-pCa relationships were fit using the equation $P/P = [Ca^{2+}]^{nH}/(k^{nH} + [Ca^{2+}]^{nH})$, where nH is the Hill coefficient and k is the $[Ca^{2+}]$ required to reach half-maximal activation (i.e., pCa_{50}).

Dynamic XB behavior was measured using a stretch activation protocol as previously described [21]. Skinned preparations were placed in Ca^{2+} solutions (pCa 6.1) that generated ~35% of maximal force and rapidly stretched by 2% of initial muscle length. The specific components of the stretch activation response have been described earlier [22,26].

2.7. Myocyte isolation and in vitro shortening and Ca^{2+} handling

Ventricular cardiomyocytes were enzymatically isolated from mouse hearts as previously described [26]. Sarcomere shortening was assessed using a video-based sarcomere length detection system (IonOptix). Ca^{2+} transients were measured from recordings in myocytes loaded with 2 μM indo-1 AM (Invitrogen) and 0.025% (wt/wt) Pluronic F-127 (Invitrogen) for 20 min at room temperature (25 °C). Sarcomere shortening and Ca^{2+} transients were measured simultaneously using 2 Hz field stimulation with 1.8 mM Ca^{2+}.

2.8. Statistical analysis

Data were analyzed using one-way analysis of variance as previously described [21], and multiple pairwise comparisons were made using Fisher's least significant difference (Fisher's LSD) method. Values are reported as means ± SEM. The criterion for statistical

significance was set at p b 0.05, and the asterisks(*) and number(#) symbols in the figures and tables denote statistical significance using post hoc Fisher's LSD comparisons.

3. Results

3.1. Effects of MYBPC3 ablation in MLP$^{-/-}$ on myocardial protein expression and phosphorylation

The expression and phosphorylation levels of MLP, cMyBPC, and other regulatory myofibrillar proteins were quantified in adult animals at age ~10 weeks. The absence of MLP and cMyBPC in each respective TG line were confirmed by western blot. Relative levels of cMyBPC were unchanged between WT and MLP$^{-/-}$ mice; levels of MLP were also unchanged between WT and MYBPC3$^{-/-}$ mice (Fig. 1A). However, there was a decrease in cMyBPC phosphorylation in the MLP$^{-/-}$ hearts (0.71 ± 0.07, p b 0.05 vs. WT)(Fig. 1B), which is consistent with previous studies that have demonstrated decreased cMyBPC phosphorylation in human and experimental HF [30,31]. No significant differences in relative phosphorylation or abundance of TnT and TnI were detected among each group compared to WT (Fig. 1B). Expression of β-myosin heavy chain (MHC) was only modestly elevated in MLP$^{-/-}$ (12.9 ± 2.5% n = 8 vs. WT 7.4 ± 1.7% n = 7, not significant) and DKO (10.5 ± 1.6% n = 7, not significant), whereas βMHC was significantly increased in MYBPC3$^{-/-}$ (15.3 ± 3.0% n = 8, p b 0.05)(Fig. 1C). We also examined relative expression levels of Ca^{2+} handling proteins and found no differences among all groups in expression of Ryr2 and Pln, as well as no differences in relative Pln p16 phosphorylation (Fig. 1D and E). HSC70, a constitutively expressed chaperone protein, was used as loading control to show equal amounts of the samples have been loaded onto the gels.

3.2. Morphologic changes in MLP$^{-/-}$ hearts after MYBPC3 deletion

Cardiac morphology was examined to determine the in vivo phenotypic effects of MLP$^{-/-}$ and MYBPC3$^{-/-}$ genetic complementation. At 10 weeks, MLP$^{-/-}$ and MYBPC3$^{-/-}$ mice developed severe cardiomegaly, whereas DKO hearts appeared to be similar in size to WT hearts (Fig. 1F). MLP$^{-/-}$ mice displayed a significant increase in heart:body weight ratio (6.81 ± 0.16 mg/g) vs WT (5.09 ± 0.23 mg/g, p b 0.05) and DKO (6.14 ± 0.15 mg/g, p b 0.05) mice (Fig. 1G). Consistent with previous findings [25,32], histological examination revealed signs of hypertrophic pathology in MLP$^{-/-}$ and MYBPC3$^{-/-}$, including myocyte disarray and fibrosis, which were less prominent in the DKO hearts (Fig. S1). Cardiac fibrosis, assessed by Masson's trichrome staining, was significantly higher in MLP$^{-/-}$ (0.43 ± 0.14% vs WT 0.05 ± 0.03%, p b 0.05) and MYBPC3$^{-/-}$ (0.46 ± 0.15%, p b 0.05) hearts but not in DKO (0.10 ± 0.06%, not significant) hearts (Fig. 1H). Similarly, IHC staining showed apparent decreases in myofilament organization in MLP$^{-/-}$ and MYBPC3$^{-/-}$ myocytes such that Z disc bands appeared distorted and poorly aligned, features which were not observed in typical WT and DKO myocytes (Fig. S2). The prevention of pathologic remodeling in DKO hearts was confirmed by echocardiography. MLP$^{-/-}$ mice had severely dilated LV chambers compared to WT, evidenced by increased end-systolic dimension (ESD) and enddiastolic dimension (EDD)(Table 1). Ventricular chamber changes were also assessed by P-V loop analysis of end-systolic (ESV) and enddiastolic (EDV) volumes and showed consistent pattern of dilation in MLP$^{-/-}$ mice and normalization in DKO mice

(Table 1). Characteristic of the DCM phenotype, the enlarged ventricular chamber was also accompanied by thinned walls in $MLP^{-/-}$ mice. In contrast, DKO mice were spared from ventricular thinning and chamber dilation. However, DKO hearts displayed modestly increased end-diastolic posterior wall thickness (PWTd) and LV mass:body weight ratio when compared to WT hearts (Table 1).

3.3. Effect of MYBPC3 ablation in $MLP^{-/-}$ mice on in vivo cardiac function

The impact of MYBPC3 ablation in the $MLP^{-/-}$ background on in vivo contractile function and hemodynamics was assessed in DKO mice by echocardiography and P-V loops. Parallel to morphologic improvements, echocardiography found that DKO had significantly increased ejection fraction (EF) and fractional shortening (FS), indicators of systolic performance that normalized to near WT levels (Table 1). EF was also assessed by P-V loop analysis (Table 1), which revealed similar normalization of EF in DKO (39.6 ± 4.2%) to WT levels (46.6 ± 5.9%). Consistent with previous reports [5], EF in $MLP^{-/-}$ mice was markedly reduced (31.1 ± 3.6% p b 0.05) compared to WT. It is interesting to note ejection time (ET) was prolonged in $MLP^{-/-}$ mice (64.25 ±2.82 ms, p b 0.05), shortened in $MYBPC3^{-/-}$ mice (38.98 ± 1.60 ms, p b 0.05), and preserved in DKO mice (48.05 ± 2.31 ms, not significant), when compared to WT mice (53.30 ± 2.62 ms). The DKO phenotype was stable and the mice live to a normal life span. Echocardiography findings in older, 6–7-month-old, DKO mice showed largely maintained EF (54.89 ± 3.07%, n = 6) and FS (27.68 ± 2.42%, n = 6), mirroring results obtained in 10 week old DKO mice.

The rate of maximal pressure development (dP/dt_{max}) was also blunted in $MLP^{-/-}$ mice (4496 ± 196 mmHg/s, p b 0.05) when compared to WT mice (7174 ± 518 mmHg/s). Deletion of MYBPC3 in the $MLP^{-/-}$ background normalized DKO dP/dt_{max} to WT levels (7851 ±505 mmHg/s), and similar to rates displayed by $MYBPC3^{-/-}$ mice(8166 ± 535 mmHg/s)(Fig. 2A and B). The time taken to reach dP/dt_{max}(t_d) was similar in WT (47.5 ± 3.2 ms) and $MLP^{-/-}$ (43.3 ± 3.5 ms) hearts but were equally accelerated in $MYBPC3^{-/-}$ (25.9 ± 1.5 ms, p b 0.05) and DKO (28.1 ± 1.1 ms, p b 0.05) hearts (Fig. 2C). The peak pressure at end systole (ESP) was significantly lower in $MLP^{-/-}$ mice (85.1 ± 2.7 mmHg vs. WT 99.8 ± 3.4 mmHg, p b 0.05). However, despite increased dP/dt_{max} and faster t_d, peak end-systolic pressure was significantly lower in DKO hearts (80.4 ± 3.1 mmHg), which may be due to the truncated ET (Fig. 2D). Additionally, P-V loop and echocardiography analysis also demonstrated significant diastolic dysfunction in all three knockout models as evidenced by elevated end-diastolic pressure (EDP), prolonged isovolumic relaxation time (IVRT), and slowed relaxation time constant (τ). However, the proportionate time spent in systole vs. diastole (S:D) in DKO (0.61 ± 0.02) was similar to WT (0.71 ± 0.03), while S:D was significantly elevated in $MLP^{-/-}$ mice (0.93 ± 0.11, p b 0.05)(Table 1).

3.4. Effect of MYBPC3 ablation in $MLP^{-/-}$ mice on steady-state force and cross-bridge kinetics

Skinned myocardium was isolated from each mouse line to determine steady-state force generation and dynamic XB kinetics. Steady-state force-pCa relations were assess by a series of slack-restretch maneuvers in pCa solutions ranging from pCa 9.0 to pCa 4.5 (Table

S1). Notably, $MLP^{-/-}$ skinned myocardium displayed significantly blunted maximal force generation in pCa 4.5 (Fig. 3A). Passive resting tension in pCa 9.0 were unchanged among all groups. The Hill coefficients (n_H) were also not different between groups, however, the Ca^{2+} sensitivity of force generation (pCa_{50}) were increased in skinned myocardium isolated from $MYBPC3^{-/-}$ and DKO hearts (Fig. 3B).

Stretch activation maneuvers at submaximal (~35% of maximal Ca^{2+} activated force) Ca^{2+} activation were used to determine dynamic strain-induced XB behavior in each group (Fig. 3C–F). The immediate rise in force (P_1), which results from stretch-induced strain of attached XBs, was not significantly different between the three knockout groups compared to WT. However, the magnitude of force per-cross-sectional-area at P1 in response to acute stretch was significantly lower in $MLP^{-/-}$ skinned preparations, consistent with our observation that $MLP^{-/-}$ skinned myocardium also displayed impaired maximal Ca^{2+}-activated force production (F_{max}) (Table S2). The rate of XB detachment, k_{rel}, was significantly slowed in the $MLP^{-/-}$ skinned preparations, and consistent with previous findings, k_{rel} was accelerated in $MYBPC3^{-/-}$ skinned preparations [22,26]. Remarkably, k_{rel} in the DKO group was completely normalized to WT levels (Fig. 3G). $MLP^{-/-}$ preparations also exhibited significantly higher minimum amplitude of force transient (P_2)(0.102 ± 0.014 vs. 0.000 ± 0.008 in WT, p b 0.05) with reduced magnitude of XB recruitment (P_{df})(0.121 ± 0.016 vs 0.208 ± 0.014 in WT, p b 0.05) (Fig. 3H). However, the rate of cooperative XB recruitment, k_{df}, was unchanged in $MLP^{-/-}$ skinned preparations. In contrast, k_{df} was significantly accelerated in $MYBPC3^{-/-}$ and DKO preparations compared to WT (Fig. 3I). Overall, the results indicate MYBPC3 ablation in the $MLP^{-/-}$ background effectively accelerates the rate of XB cycling and enhances the magnitude of XB recruitment.

3.5. Isolated myocyte contractile function and Ca^{2+} handling properties

To determine if Ca^{2+} handling contributed to DKO rescue of DCM phenotype, we assessed in vitro unloaded myocyte contractile and Ca^{2+} handling properties. We did not detect differences in resting Ca^{2+} levels across all groups (Table S3). The peak Ca^{2+} amplitude after stimulation was elevated in the $MLP^{-/-}$ myocytes (27 ± 1.5 AU vs. WT 21.3 ±1.5 AU, p b 0.05). Resting sarcomere length was significantly decreased in $MYBPC3^{-/-}$ (1.71 ± 0.01 μm) and DKO (1.73 ± 0.01 μm), when compared to WT (1.80 ± 0.01 μm).

4. Discussion

Impaired contractile function at the myofilament level is a key component driving the progression to heart failure. Typically, mutations of genes that enhance contractility lead to HCM, whereas those that reduce contractility lead to DCM [12,14]. In this study, we provide evidence of the utility of targeting the sarcomere to normalize cardiac contractility and thereby protect the heart from pathologic hypertrophy.

4.1. MYBPC3 ablation improves in vivo contractile function in a murine model of DCM

Force development during early systole is heavily dependent on the cooperative recruitment of force generating XBs to the thin filament [33]. In an intact heart, enhancements of thin filament activation and ventricular contractility can be measured as increases to dP/dt_{max},

and reduced time required to reach dP/dt_{max} (t_d). In particular, t_d has been demonstrated to be inversely proportional to cardiac contractile state and independent of preload conditions [34], which is an important consideration given the ventricular chamber dilation in $MLP^{-/-}$ and $MYBPC3^{-/-}$ hearts. The accelerated rates of force development (Fig. 2B) and decreased t_d (Fig. 2C) in DKO mice indicate an increase in contractility, likely a result of removing cMyBPC constraint in the sarcomere was sufficient to increase overall cardiac contractility. These results are consistent with previous studies showing cMyBPC as an important modulator of the rate of force development, accelerating dP/dt_{max} in a phosphorylation dependent manner [35]. The effect of MYBPC3 ablation is thought to be similar to cMyBPC phosphorylation, as both conditions remove constraints on XB recruitment, thereby accelerating the rate of force development. Thus, our results demonstrate a dominant effect of contractility on cardiac remodeling, resulting in the relative normalization of DKO LV chamber dimension and wall thicknesses (Table 1).

While it is difficult to separate systolic and diastolic effects, especially in advance disease states, DCM has been widely considered to be caused by impaired systolic function whereas HCM predominately result from diastolic dysfunction. Interestingly, the protective effects of enhanced systolic contractility appear to overcome significant diastolic dysfunction in DKO mice and prevent eccentric remodeling. One possible explanation for this effect is the normalized balance of times spent in systole vs. diastole during each cardiac cycle contributed to the improved overall cardiac function in DKO mice, despite prolongation of diastole. Elevated systolic to diastolic duration (S:D) ratio, has been used as an indicator of global cardiac performance and has been associated with adverse outcomes in patients with DCM [36]. Taken together, the improved systolic rate of pressure development and normalized S:D duration ratio in DKO was able to achieve an overall beneficial effect on cardiac function and blunt pathologic remodeling, as evidenced by reduction of hypertrophy and fibrosis (Fig. 1F–H).

Contractile dysfunction can also arise due to impairments in Ca^{2+} cycling, since the availability of Ca^{2+} modulates the magnitude and kinetics of myofilament activation. The importance of Ca^{2+} handling in pathogenesis have been highlighted by studies that have rescued models of DCM and HCM by enhanced sarcoplasmic reticulum (SR) Ca^{2+} uptake [32,37]. However, evidence of Ca^{2+} handling dysfunction in the $MLP^{-/-}$ model have been mixed. Studies have reported decreased SR Ca^{2+} content and amplitude of Ca^{2+} transients in intact myocytes [32,38], while others have reported higher [39] or unchanged [40] Ca^{2+} transients and SR Ca^{2+} stores. In experiments with unloaded intact myocytes (Table S3), we observed an increase in peak Ca^{2+} transient in $MLP^{-/-}$ myocytes, with no changes in baseline Ca^{2+} across the groups. Whereas the lower relative peak Ca^{2+} transients in DKO myocytes in comparison to $MLP^{-/-}$ myocytes would be expected to result in reduced contractility, the opposite was true. Furthermore, we did not detect differences in the expression and phosphorylation in Ryr2 and Pln (Fig. 1D and E). Therefore, it is unlikely the functional improvements in DKO mice can be attributed to enhancements in Ca^{2+} cycling. Instead, improved contractile performance in DKO myocardium is expected to primarily involve differences in myofilament function.

4.2. MYBPC3 ablation enhances in vitro contractile function in a murine model of DCM

Earlier efforts to improve and/or reverse cardiac myocyte dysfunction in the MLP deficient murine model of DCM have focused on ablation of specific proteins that are involved in Ca^{2+} handling (phospholamban), Z-disc adapter proteins (cardiac specific ankyrin repeat protein), and β2-adrenergic receptors [32,41–43]. Recently, efforts to improve cardiac myocyte contractile function in heart failure have expanded to include direct manipulation of the force-generating acto-myosin XB [16,44]. Thus, in this study we tested whether modulating the rate and magnitude of acto-myosin XB formation, by MYBPC3 ablation, can improve in vivo contractile function in a murine model of DCM caused by MLP deletion.

Consistent with our results, previous studies have shown that at the myofilament level, MLP deletion decreases maximal force generation [9] and alters Ca^{2+} cycling [39]. In this study, we also showed that MLP deletion led to hypocontractile XB behavior as demonstrated by slowing of XB detachment and reduction of XB recruitment magnitude during contractile activation (Fig. 3, Table S2). The MLP-deletion induced hypocontractile XB behavior and reduced force generation may be due to a combination of primary and compensatory changes linked to cytoskeletal disorganization that prevents proper transduction of external loads at the level of Z-discs within the sarcomere [10,45]. Here, we found MYBPC3 deletion in $MLP^{-/-}$ ameliorated defects in maximal Ca^{2+} activated force (F_{max}), a measure of total available XBs and adequate cellular integrity to transmit such force. The increased F_{max} in DKO preparations to WT levels is likely a result of freeing additional myosin binding sites on actin that would otherwise be bound to cMyBPC, which allows for recruitment of additional XBs. These additionally available XBs would be expect to contribute to the normalization of DKO maximal cardiac pressure generation, dP/dt_{max}. DKO myocardial contractility enhancements can also be attributed to the MYBPC3 ablation induced acceleration of the rates of XB detachment (k_{rel}) and recruitment (k_{df}) during Ca^{2+} activation [22,28,46]. It is now accepted that removal of the physical constraints imposed by cMyBPC on myosin heads, via MYBPC3 ablation, shifts the net equilibrium of myosin heads towards actin binding sites on the thin filament [24,47]. Thus, at submaximal levels of activating Ca^{2+}, the rate of XB detachment (k_{rel}) and the magnitude of XB recruitment, P_{df}, were enhanced in DKO myocardium to match WT levels. Because the rate of XB detachment is the rate limiting step of XB turnover in a two-state XB model [48], enhanced XB detachment would be expected to increase overall XB turnover and accelerate myocardial contractility and pressure development, which correlates with the normalized DKO t_d and ET at the whole heart level. The higher level of P2 and resultant reduction in P_{df} in $MLP^{-/-}$ skinned myocardium may be directly related to slower k_{rel}, which would delay XB detachment and consequently limit the number of open actin-binding sites available for newly recruited myosin XBs. MLP ablation did not affect the rate of delayed XB recruitment (i.e., k_{df}), but MYBPC3 ablation significantly accelerated k in the $MYBPC3^{-/-}$ df and DKO groups. Taken together, our data explains, at the myofilament level, the increased in vivo contractility in DKO mice. However, the elimination of cMyBPC would be expected to decrease the ability of the heart to access its contractile reserve, such as protein kinase A mediated acceleration of contractile kinetics [33]. Thus, a significant disadvantage of MYBPC3 ablation in DKO hearts is limited cardiac reserve, which would result in adverse responses to additional stressors.

We found cMyBPC phosphorylation was reduced in $MLP^{-/-}$ hearts (Fig. 1B), and because cMyBPC phosphorylation is known to accelerate XB kinetics and help maintain cardiac output during conditions of cardiac stress, but is known to become dephosphorylated in HF [30,31], cMyBPC dephosphorylation in $MLP^{-/-}$ myocardium may contribute to contractile dysfunction. Another contributor to slow contractile kinetics is changes in relative βMHC expression, which inherently possesses slower ATPase enzymatic kinetics compared to αMHC [49]. But this iso-form shift is thought to be a part of compensatory mechanisms to HF and is most likely unrelated to the primary MLP-deficiency induced contractile deficits. The relatively minor changes in αMHC expression would not be expected to contribute significantly to the improvements we observed in cardiac systolic function in DKO mice.

5. Strengths and limitations

In our study, the major limitation of the “rescue” phenotype in DKO mouse is the persistence of reduced diastolic capacity. This deficit may be a result of the use of MYBPC3 ablation to overtly increase contractility. It has been noted that diastolic dysfunction is a primary component of preclinical HCM [50], and because DKO hearts showed features of concentric hypertrophy (increased wall thickness compared to WT), it may be that the DKO mice have a mild form of HCM induced by excess hypercontractility in the absence of cMyBPC. This suggests $MLP^{-/-}$ and DKO mice have disparate mechanisms causing diastolic dysfunction and requires additional studies to better understand such differences.

Contrary to the “double dose gene effect” principle, which postulates multiple disease-associated mutations are additive and lead to more severe phenotype and prognosis, the combination of hypo- and hyper-contractile inducing gene ablations in DKO mice greatly reduced the severity of whole-heart and cardiomyocyte contractile dysfunction. Patients with similar cases of complementary compound or double mutation would be rare since their phenotypes may be mild or subclinical, but may explain extensive heterogeneity in penetrance among known cardiomyopathy associated mutations.

6. Conclusion

In summary, our results indicate that myofilament contractility can be a key determinant of directionality of pathologic remodeling. MYBPC3 ablation has a net dominant effect on myofilament contractile behavior and offsets the hypocontractile kinetics observed in myocardium lacking MLP, leading to largely normalized sarcomeric and whole heart function. Of clinical significance, our sarcomeric manipulation demonstrates that increasing the reduced force production of hypocontractile-causing mutations can be an effective treatment strategy. Our approach uses MYBPC3 ablation as a means of increasing myofilament power output, but this strategy is broadly applicable to other specific components of the sarcomere. If the effects of a mutation on myocardial contractility can be identified, precise modifiers of sarcomeric force output can be used to reverse the contractility deficit and therefore interrupt pathologic remodeling.

Supplementary Material

Refer to Web version on PubMed Central for supplementary material.

Acknowledgements

We would like to thank Xiaoqin Chen, MD, Department of Physiology and Biophysics at Case Western Reserve University for assistance with echocardiography and the Tissue Resources Core Facility of the Case Comprehensive Cancer Center (P30CA043703) for assistance with histology.

Funding

This work was supported by the National Institutes of Health, United States (T32-HL007567, R01-HL-114770, T32-GM007250, S10-OD012635) and the American Heart Association, United States (16POST30730000).

Abbreviations

cMyBPC	cardiac myosin binding protein C
dP/dt_{max}	peak rate of left ventricular pressure development
EDP	end-diastolic pressure
EF	ejection fraction
ESP	end-systolic pressure
F_{max}	maximum Ca^{2+} max activated force
F_{min}	Ca^{2+} independent force
FS	fractional shortening
H&E	hematoxylin and eosin stain
HR	heart rate
HSC70	heat shock chaperone 70
IVRT	isovolumic relaxation time
k_{df}	rate constant of delayed force development
k_{rel}	rate constant of force decay
LV	left ventricle
n_H	Hill coefficient
NTG	non-transgenic
pCa_{50}	[Ca2+] required for 50%-maximum activation
PKA	protein kinase A
P	submaximal force

Pln	phospholamban
P_o	maximal force
P-V	pressure-volume
RyR	ryanodine receptor
SL	sarcomere length
τ	rate constant of pressure relaxation
TnI	troponin I
TnT	troponin T
XB	cross-bridge

References

[1]. Tayal U, Prasad S, Cook SA, Genetics and genomics of dilated cardiomyopathy and systolic heart failure, Gend. Med 9 (2017) 20, 10.1186/s13073-017-0410-8.

[2]. Mcnally EM, Golbus JR, Puckelwartz MJ, Genetic mutations and mechanisms in dilated cardiomyopathy, J. Clin. Invest 123 (2013) 19–26, 10.1172/JCI62862.the. [PubMed: 23281406]

[3]. Hinson JT, Chopra A, Nafissi N, Polacheck WJ, Benson CC, Swist S, Gorham J, Yang L, Schafer S, Sheng CC, Haghighi A, Homsy J, Hubner N, Church G, Cook SA, Linke WA, Chen CS, Seidman JG, Seidman CE, Titin mutations in iPS cells define sarcomere insufficiency as a cause of dilated cardiomyopathy, Science 349 (2015) 982–986, 10.1126/science.aaa5458(80-.). [PubMed: 26315439]

[4]. Burke MA, Cook SA, Seidman JG, Seidman CE, Clinical and mechanistic insights into the genetics of cardiomyopathy, J. Am. Coll. Cardiol 68 (2016) 2871–2886, 10.1016/j.jacc.2016.08.079. [PubMed: 28007147]

[5]. Arber S, Hunter JJ, Ross J, Hongo M, Sansig G, Borg J, Perriard J-C, Chien KR, Caroni P, MLP-deficient mice exhibit a disruption of cardiac cytoarchitectural organization, dilated cardiomyopathy, and heart failure, Cell 88 (1997) 393–403, 10.1016/S0092-8674(00)81878-4. [PubMed: 9039266]

[6]. Geier C, Gehmlich K, Ehler E, Hassfeld S, Perrot A, Hayess K, Cardim N, Wenzel K, Erdmann B, Krackhardt F, Posch MG, Bublak A, Nägele H, Scheffold T, Dietz R, Chien KR, Spuler S, Fürst DO, Nürnberg P, Özcelik C, Beyond the sarcomere: CSRP3 mutations cause hypertrophic cardiomyopathy, Hum. Mol. Genet 17 (2008) 2753–2765, 10.1093/hmg/ddn160. [PubMed: 18505755]

[7]. Mohapatra B, Jimenez S, Lin JH, Bowles KR, Coveler KJ, Marx JG, Chrisco MA, Murphy RT, Lurie PR, Schwartz RJ, Elliott PM, Vatta M, McKenna W, Towbin JA, Bowles NE, Mutations in the muscle LIM protein and α-actinin-2 genes in dilated cardiomyopathy and endocardial fibroelastosis, Mol. Genet. Metab 80 (2003) 207–215, 10.1016/S1096-7192(03)00142-2. [PubMed: 14567970]

[8]. Bos JM, Poley RN, Ny M, Tester DJ, Xu X, Vatta M, Towbin JA, Gersh BJ, Ommen SR, Ackerman MJ, Genotype-phenotype relationships involving hypertrophic cardiomyopathy-associated mutations in titin, muscle LIM protein, and telethonin, Mol. Genet. Metab 88 (2006) 78–85, 10.1016/j.ymgme.2005.10.008. [PubMed: 16352453]

[9]. Unsld B, Schotola H, Jacobshagen C, Seidler T, Sossalla S, Emons J, Klede S, Knll R, Guan K, El-Armouche A, Linke WA, Kgler H, Hasenfuss G, Age-dependent changes in contractile function and passive elastic properties of myocardium from mice lacking muscle LIM protein (MLP), Eur. J. Heart Fail 14 (2012) 430–437, 10.1093/eurjhf/hfs020. [PubMed: 22371524]

[10]. Flick MJ, Konieczny SF, The muscle regulatory and structural protein MLP is a cytoskeletal binding partner of betaI-spectrin, J. Cell Sci 113 (2000) 1553–1564. [PubMed: 10751147]

[11]. Spudich JA, Hypertrophic and dilated cardiomyopathy: four decades of basic research on muscle lead to potential therapeutic approaches to these devastating genetic diseases, Biophys. J 106 (2014) 1236–1249, 10.1016/j.bpj.2014.02.011. [PubMed: 24655499]

[12]. Moore JR, Leinwand L, Warshaw DM, Understanding cardiomyopathy pheno-types based on the functional impact of mutations in the myosin motor, Circ. Res 111 (2012) 375–385, 10.1161/CIRCRESAHA.110.223842. [PubMed: 22821910]

[13]. Alcalai R, Seidman JG, Seidman CE, Genetic basis of hypertrophic cardiomyopathy: from bench to the clinics, J. Cardiovasc. Electrophysiol 19 (2008) 104–110, 10.1111/j.1540-8167.2007.00965.x. [PubMed: 17916152]

[14]. Davis J, Davis LC, Correll RN, Makarewich CA, Schwanekamp JA, Moussavi-Harami F, Wang D, York AJ, Wu H, Houser SR, Seidman CE, Seidman JG, Regnier M, Metzger JM, Wu JC, Molkentin JD, A tension-based model distinguishes hypertrophic versus dilated cardiomyopathy, Cell 165 (2016) 1147–1159, 10.1016/j.cell.2016.04.002. [PubMed: 27114035]

[15]. Chen PP, Patel JR, a Powers P, Fitzsimons DP, Moss RL, Dissociation of structural and functional phenotypes in cardiac myosin-binding protein C conditional knockout mice, Circulation 126 (2012) 1194–1205, 10.1161/CIRCULATIONAHA.111.089219. [PubMed: 22829020]

[16]. Teerlink JR, Clarke CP, Saikali KG, Lee JH, Chen MM, Escandon RD, Elliott L, Bee R, Habibzadeh MR, Goldman JH, Schiller NB, Malik FI, Wolff AA, Dose-dependent augmentation of cardiac systolic function with the selective cardiac myosin activator, omecamtiv mecarbil: a first-in-man study, Lancet 378 (2011) 667–675, 10.1016/S0140-6736(11)61219-1. [PubMed: 21856480]

[17]. Mearini G, Stimpel D, Geertz B, Weinberger F, Krämer E, Schlossarek S, Mourot-Filiatre J, Stoehr A, Dutsch A, Wijnker PJM, Braren I, a Katus H, Müller OJ, Voit T, Eschenhagen T, Carrier L, Mybpc3 gene therapy for neonatal cardiomyopathy enables long-term disease prevention in mice, Nat. Commun 5 (2014) 5515, 10.1038/ncomms6515. [PubMed: 25463264]

[18]. Malik FI, Hartman JJ, A Elias K, Morgan BP, Rodriguez H, Brejc K, Anderson RL, Sueoka SH, Lee KH, Finer JT, Sakowicz R, Baliga R, Cox DR, Garard M, Godinez G, Kawas R, Kraynack E, Lenzi D, Lu PP, Muci A, Niu C, Qian X, Pierce DW, Pokrovskii M, Suehiro I, Sylvester S, Tochimoto T, Valdez C, Wang W, Katori T, A Kass D, Shen Y-T, Vatner SF, Morgans DJ, Cardiac myosin activation: a potential therapeutic approach for systolic heart failure, Science 331 (2011) 1439–1443, 10.1126/science.1200113. [PubMed: 21415352]

[19]. Davis J, Westfall MV, Townsend D, Blankinship M, Herron TJ, Guerrero-Serna G, Wang W, Devaney E, Metzger JM, Designing heart performance by gene transfer, Physiol. Rev 88 (2008) 1567–1651, 10.1152/physrev.00039.2007. [PubMed: 18923190]

[20]. Kim DH, Chien F-J, Eisen HJ, Pharmacologic management for heart failure and emerging therapies, Curr. Cardiol. Rep 19 (2017) 94, 10.1007/s11886-017-0899-x. [PubMed: 28840572]

[21]. Mamidi R, Gresham KS, Li A, dos Remedios CG, Stelzer JE, Molecular effects of the myosin activator omecamtiv mecarbil on contractile properties of skinned myocardium lacking cardiac myosin binding protein-C, J. Mol. Cell. Cardiol 85 (2015) 262–272, 10.1016/j.yjmcc.2015.06.011. [PubMed: 26100051]

[22]. Stelzer JE, Dunning SB, Moss RL, Ablation of cardiac myosin-binding protein-C accelerates stretch activation in murine skinned myocardium, Circ. Res 98 (2006) 1212–1218, 10.1161/01.RES.0000219863.94390.ce. [PubMed: 16574907]

[23]. Tong CW, Stelzer JE, Greaser ML, a Powers P, Moss RL, Acceleration of crossbridge kinetics by protein kinase A phosphorylation of cardiac myosin binding protein C modulates cardiac function, Circ. Res 103 (2008) 974–982, 10.1161/CIRCRESAHA.108.177683. [PubMed: 18802026]

[24]. Colson BA, Patel JR, Chen PP, Bekyarova T, Abdalla MI, Tong CW, Fitzsimons DP, Irving TC, Moss RL, Myosin binding protein-C phosphorylation is the principal mediator of protein kinase A effects on thick filament structure in myocardium, J. Mol. Cell. Cardiol 53 (2012) 609–616, 10.1016/j.yjmcc.2012.07.012. [PubMed: 22850286]

[25]. Harris SP, Bartley CR, Hacker TA, McDonald KS, Douglas PS, Greaser ML, Powers PA, Moss RL, Hypertrophic cardiomyopathy in cardiac myosin binding protein-C knockout mice, Circ. Res 90 (2002) 594–601, 10.1161/01.RES.0000012222.70819.64. [PubMed: 11909824]

[26]. Cheng Y, Wan X, a McElfresh T, Chen X, Gresham KS, Rosenbaum DS, Chandler MP, Stelzer JE, Impaired contractile function due to decreased cardiac myosin binding protein C content in the sarcomere, Am. J. Physiol. Heart Circ. Physiol 305 (2013) H52–H65, 10.1152/ajpheart.00929.2012. [PubMed: 23666674]

[27]. Kennedy DJ, Vetteth S, Periyasamy SM, Kanj M, Fedorova L, Khouri S, Kahaleh MB, Xie Z, Malhotra D, Kolodkin NI, Lakatta EG, Fedorova OV, Bagrov AY, Shapiro JI, Central role for the cardiotonic steroid marinobufagenin in the pathogenesis of experimental uremic cardiomyopathy, Hypertension 47 (2006) 488–495, 10.1161/01.HYP.0000202594.82271.92. [PubMed: 16446397]

[28]. Gresham KS, Mamidi R, Stelzer JE, The contribution of cardiac myosin binding protein-c Ser282 phosphorylation to the rate of force generation and in vivo cardiac contractility, J. Physiol 592 (2014) 3747–3765, 10.1113/jphysiol.2014.276022. [PubMed: 24951619]

[29]. Ford SJ, Chandra M, Mamidi R, Dong W, Campbell KB, Model representation of the nonlinear step response in cardiac muscle, J. Gen. Physiol 136 (2010) 159–177, 10.1085/jgp.201010467. [PubMed: 20660660]

[30]. El-Armouche A, Pohlmann L, Schlossarek S, Starbatty J, Yeh YH, Nattel S, Dobrev D, Eschenhagen T, Carrier L, Decreased phosphorylation levels of cardiac myosin-binding protein-C in human and experimental heart failure, J. Mol. Cell. Cardiol 43 (2007) 223–229, 10.1016/j.yjmcc.2007.05.003. [PubMed: 17560599]

[31]. Copeland O, Sadayappan S, Messer AE, Steinen GJM, van der Velden J, Marston SB, Analysis of cardiac myosin binding protein-C phosphorylation in human heart muscle, J. Mol. Cell. Cardiol 49 (2010) 1003–1011, 10.1016/j.yjmcc.2010.09.007. [PubMed: 20850451]

[32]. Minamisawa S, Hoshijima M, Chu G, Ward CA, Frank K, Gu Y, Martone ME, Wang Y, Ross J, Kranias EG, Giles WR, Chien KR, Chronic phospholamban sarcoplasmic reticulum calcium ATPase interaction is the critical calcium cycling defect in dilated cardiomyopathy, Cell 99 (1999) 313–322, 10.1016/S0092-8674(00)81662-1. [PubMed: 10555147]

[33]. Mamidi R, Gresham KS, Li J, Stelzer JE, Cardiac myosin binding protein-C Ser(302) phosphorylation regulates cardiac β-adrenergic reserve, Sci. Adv (3) (2017), e1602445 10.1126/sciadv.1602445. [PubMed: 28345052]

[34]. Adler D, Et A, Erratum: Time to dp/dt(max), a preload-independent index of contractility: Open-chest dog study, Basic Res. Cardiol 91 (94–100) (1996) 267, 10.1007/BF00788913.

[35]. Gresham KS, Mamidi R, Li J, Kwak H, Stelzer JE, Sarcomeric protein modification during adrenergic stress enhances cross-bridge kinetics and cardiac output, J. Appl. Physiol 122 (2017) 520–530, 10.1152/japplphysiol.00306.2016. [PubMed: 27909224]

[36]. Mondal T, Slorach C, Manlhiot C, Hui W, Kantor PF, McCrindle BW, Mertens L, Friedberg MK, Prognostic implications of the systolic to diastolic duration ratio in children with idiopathic or familial dilated cardiomyopathy, Circ. Cardiovasc. Imaging 7 (2014) 773–780, 10.1161/CIRCIMAGING.114.002120. [PubMed: 25140066]

[37]. Peña JR, Szkudlarek AC, Warren CM, Heinrich LS, Gaffin RD, Jagatheesan G, del Monte F, Hajjar RJ, Goldspink PH, Solaro RJ, Wieczorek DF, Wolska BM, Neonatal gene transfer of Serca2a delays onset of hypertrophic remodeling and improves function in familial hypertrophic cardiomyopathy, J. Mol. Cell. Cardiol 49 (2010) 993–1002, 10.1016/j.yjmcc.2010.09.010. [PubMed: 20854827]

[38]. Esposito G, Santana LF, Dilly K, Cruz JD, Mao L, Lederer WJ, Rockman HA, Cellular and functional defects in a mouse model of heart failure, Am. J. Physiol. Heart Circ. Physiol 279 (2000) H3101–H3112, 10.1152/ajpheart.2000.279.6.H3101. [PubMed: 11087268]

[39]. Su Z, Yao A, Zubair I, Sugishita K, Ritter M, Li F, Hunter JJ, Chien KR, Barry WH, Effects of deletion of muscle LIM protein on myocyte function, Am. J. Physiol. Heart Circ. Physiol 280 (2001) H2665–H2673. [PubMed: 11356623]

[40]. Antoons G, Vangheluwe P, Volders PGA, Bito V, Holemans P, Ceci M, Wuytack F, Caroni P, Mubagwa K, Sipido KR, Increased phospholamban phosphorylation limits the force-frequency response in the MLP−/−mouse with heart failure, J. Mol. Cell. Cardiol 40 (2006) 350–360, 10.1016/j.yjmcc.2005.12.002. [PubMed: 16427649]

[41]. Lange S, Gehmlich K, Lun AS, Blondelle J, Hooper C, Dalton ND, Alvarez EA, Zhang X, Bang ML, Abassi YA, Dos Remedios CG, Peterson KL, Chen J, Ehler E, MLP and CARP are linked to chronic PKCα signalling in dilated cardiomyopathy, Nat. Commun 7 (2016) 1–11, 10.1038/ncomms12120.

[42]. Fajardo G, Zhao M, Urashima T, Farahani S, Hu D-Q, Reddy S, Bernstein D, Deletion of the β2-adrenergic receptor prevents the development of cardiomyopathy in mice, J. Mol. Cell. Cardiol 63 (2013) 155–164, 10.1016/j.yjmcc.2013.07.016. [PubMed: 23920331]

[43]. Heineke J, Wollert KC, Osinska H, Sargent MA, York AJ, Robbins J, Molkentin JD, Calcineurin protects the heart in a murine model of dilated cardiomyopathy, J. Mol. Cell. Cardiol 48 (2010) 1080–1087, 10.1016/j.yjmcc.2009.10.012. [PubMed: 19854199]

[44]. Mamidi R, Li J, Gresham KS, Verma S, Doh CY, Li A, Lal S, Dos Remedios CG, Stelzer JE, Dose-dependent effects of the myosin activator omecamtiv mecarbil on cross-bridge behavior and force generation in failing human myocardium, Circ. Heart Fail 10 (2017)10.1161/CIRCHEARTFAILURE.117.004257.

[45]. Vafiadaki E, Arvanitis DA, Sanoudou D, Muscle LIM protein: master regulator of cardiac and skeletal muscle functions, Gene 566 (2015) 1–7, 10.1016/j.gene.2015.04.077. [PubMed: 25936993]

[46]. Moss RL, Fitzsimons DP, Ralphe JC, Cardiac MyBP-C regulates the rate and force of contraction in mammalian myocardium, Circ. Res 116 (2015) 183–192, 10.1161/CIRCRESAHA.116.300561. [PubMed: 25552695]

[47]. Colson BA, Bekyarova T, Locher MR, Fitzsimons DP, Irving TC, Moss RL, Protein kinase a-mediated phosphorylation of cmybp-c increases proximity of myosin heads to actin in resting myocardium, Circ. Res 103 (2008) 244–251, 10.1161/CIRCRESAHA.108.178996. [PubMed: 18599866]

[48]. Hinken AC, Solaro RJ, A dominant role of cardiac molecular motors in the intrinsic regulation of ventricular ejection and relaxation, Physiology (Bethesda) 22 (2007) 73–80, 10.1152/physiol.00043.2006. [PubMed: 17420299]

[49]. Palmer BM, Thick filament proteins and performance in human heart failure, Heart Fail. Rev 10 (2005) 187–197, 10.1007/s10741-005-5249-1. [PubMed: 16416042]

[50]. Michels M, Soliman OII, Kofflard MJ, Hoedemaekers YM, Dooijes D, Majoor-Krakauer D, ten Cate FJ, Diastolic abnormalities as the first feature of hypertrophic cardiomyopathy in Dutch myosin-binding protein C founder mutations, JACC Cardiovasc. Imaging 2 (2009) 58–64, 10.1016/j.jcmg.2008.08.003. [PubMed: 19356534]

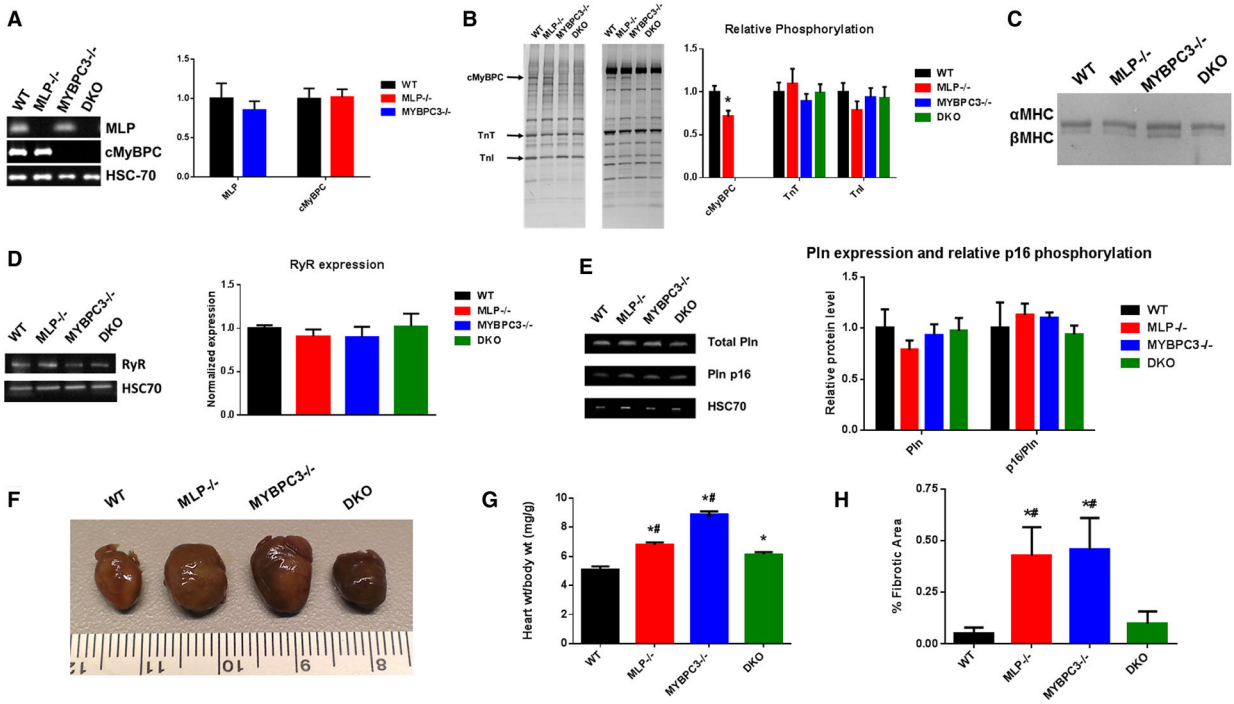

Fig. 1.

Expression and phosphorylation of myocardial proteins and myocardial morphology. (A) Western blots showing the quantification of cMyBPC and MLP levels in WT, MLP $^{-/-}$,MYBPC3$^{-/-}$, and DKO myocardial preparations. (n = 5) (B) Pro-Q and coomassie gels showing the relative phosphorylation levels of key myofilament proteins in WT, MLP $^{-/-}$,MYBPC3$^{-/-}$, and DKO myocardial preparations. cMyBPC, cardiac myosin binding protein C; TnT, troponin T; TnI, troponin I. (n = 7) (C) Representative 5% Tris-HCl gel, stained with silver stain, showing MHC isoform expression in WT, MLP$^{-/-}$,MYBPC3$^{-/-}$, andDKOmyocardialsamples. (D)Representative Western blots (left) and quantification (right) of ryanodine receptor 2 (Ryr2) and heat shock chaperone 70 (HSC70); from 8 hearts per group. (E) Representative Western blots (left) and quantification (right) of phospholamban (Pln), Pln phosphorylated at Ser16 (Pln p16), and HSC70; from 6 hearts per group. All expression were normalized to HSC70. Relative phosphorylation in B and E are normalized to total protein (i.e. phosphorylated TnT/total TnT). (F) Gross images of the hearts demonstrating dilated and hypertrophic phenotypes in MLP$^{-/-}$ and MYBPC3$^{-/-}$ groups, respectively. Scale ruler in centimeter. (G) Quantification of heart (wet weight) to body weight ratio in WT, MLP$^{-/-}$, MYBPC3$^{-/-}$, and DKO groups. (n = 7–9). (H) Quantification of fibrosis from Masson's trichrome cardiac sections, analyzed from four or five mice per group. Values are expressed as mean ± SEM. *Significantly different from WT (p b 0.05), #Significantly different from DKO (p b 0.05).

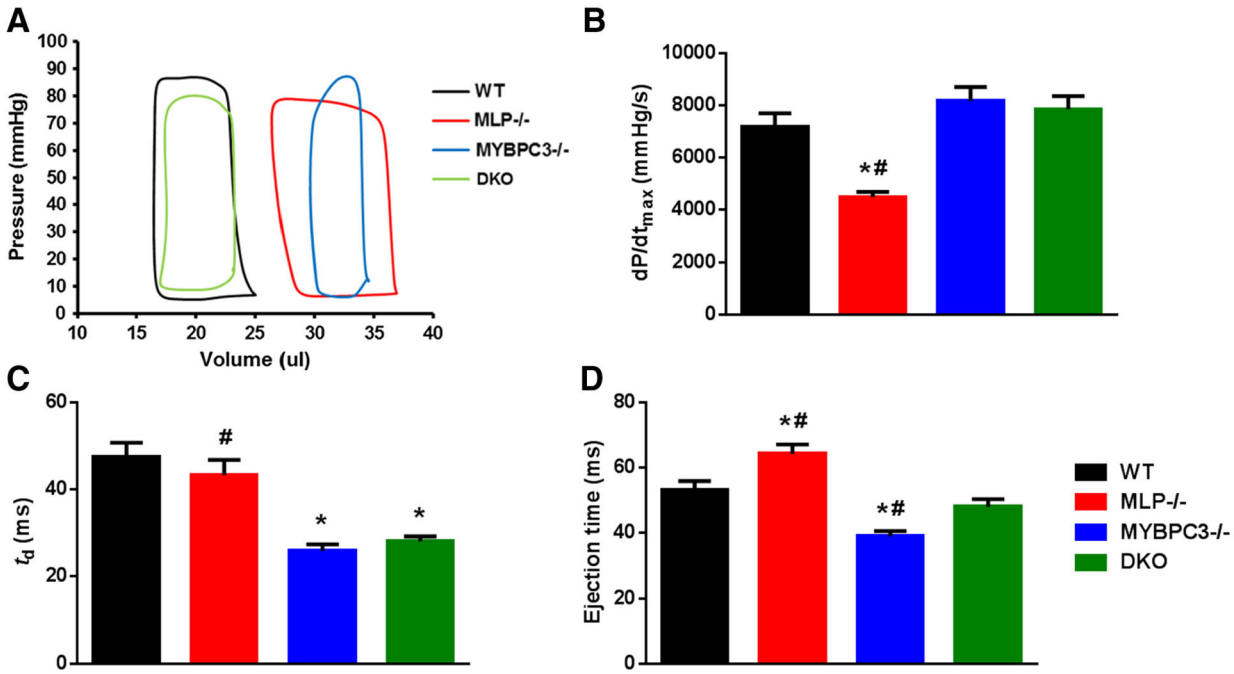

Fig. 2.

Left ventricular hemodynamic parameters measured by pressure-volume (P-V) loop analysis. (A) Representative traces from in vivo P-V measurements performed on WT, MLP $^{-/-}$, MYBPC3$^{-/-}$, and DKO hearts. (B) Quantification of the maximum rate of pressure development during systole in WT, MLP$^{-/-}$, MYBPC3$^{-/-}$, and DKO hearts. (C) Time required to reach peak pressure development during systole in WT, MLP$^{-/-}$, MYBPC3$^{-/-}$, and DKO hearts. (D) Ejection time measured in WT, MLP$^{-/-}$, MYBPC3$^{-/-}$, and DKO hearts. Values are expressed as mean ± S.E.M. from 6 to 9 mice in each group. *Significantly different from WT (p b 0.05), #Significantly different from DKO (p b 0.05).

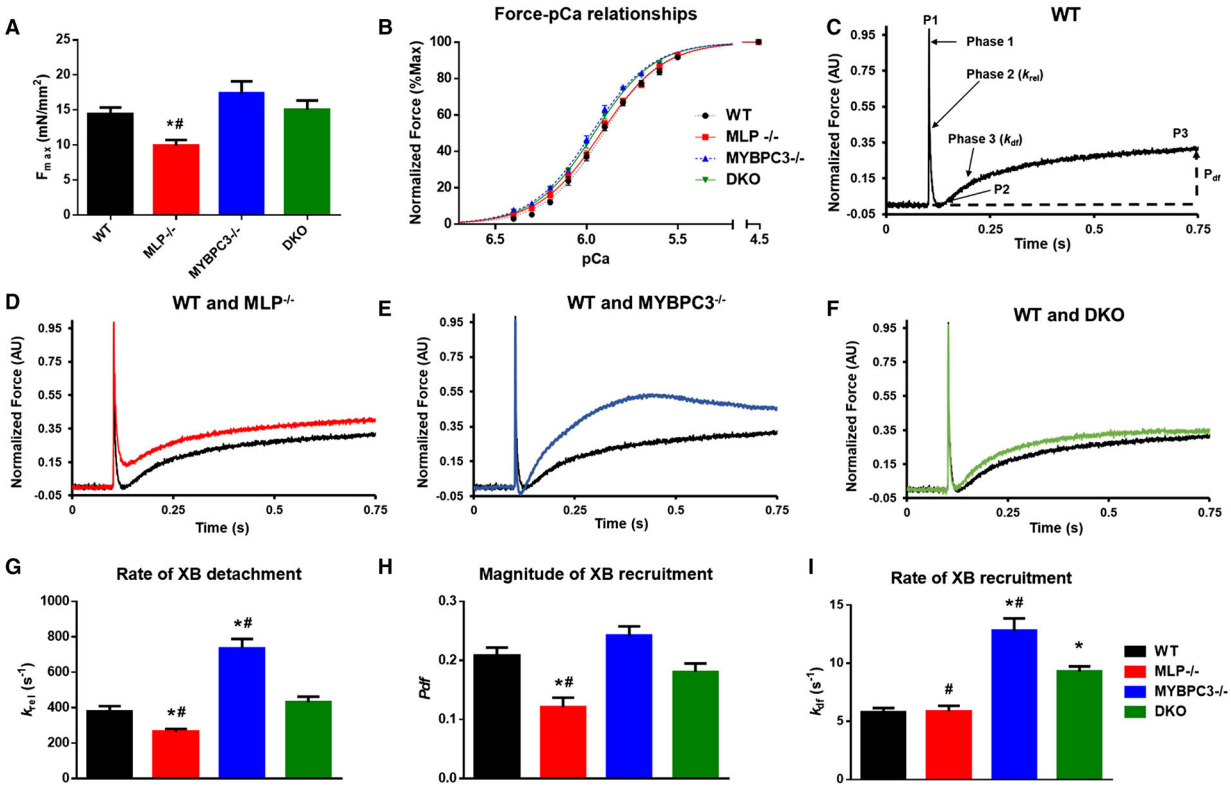

Fig. 3.

Ca^{2+}-activated force-pCa_{50} relationship and cross-bridge kinetics in skinned myocardium: (A) Ca^{2+}-activated maximal force production in skinned myocardium prepared from WT, $MLP^{-/-}$,$MYBPC3^{-/-}$, andDKOhearts. (B) Force-pCa relationships in skinned myocardium prepared from WT, $MLP^{-/-}$,$MYBPC3^{-/-}$, and DKO hearts. pCa_{50} is significantly higher in $MYBPC3^{-/-}$, and DKO myocardium when compared to the WT myocardium. (C) Representative stretch activation response in WT myocardium highlighting the important phases of the force transients and various stretch activation parameters that are measured from force responses to 2% stretch in muscle length. (D-F) Comparative representative stretch activation responses in WT and each respective knock-out myocardium showing (D) slowing of XB detachment in $MLP^{-/-}$ myocardium when compared to WT myocardium, (E) acceleration of both XB detachment and recruitment in $cMyBPC^{-/-}$ myocardium when compared to WT myocardium, and (F) normalization of XB detachment in DKO myocardium when compared to WT myocardium. Stretch-activation measurements were made in the skinned ventricular preparations using a sudden 2% stretch in muscle length to measure (G) the rate of XB detachment, k_{rel}; (H) the magnitude of overall XB recruitment in response to stretch in muscle length; P_{df}, and (I) the rate of XB recruitment; k in WT, $MLP^{-/-}$, $MYBPC3^{-/-}$ df, and DKO myocardial preparations. k_{rel} was slower in $MLP^{-/-}$ myocardium but was normalized in the DKO myocardium. Similarly, P_{df} was lower in the $MLP^{-/-}$ myocardium but was normalized in the DKO myocardium which is likely due to increased magnitude of XB recruitment in the DKO myocardium. 24 skinned myocardial

preparations from 8 to 9 hearts were used for all the groups. *Significantly different from WT (p b 0.05), #Significantly different from DKO (p b 0.05).

Table 1

LV morphology and in vivo cardiac performance measured by echocardiography and pressure-volume loop analysis.

	Echocardiography assessment			
	WT (n = 7)	MLP$^{-/-}$ (n = 7)	MYBPC3$^{-/-}$ (n = 7)	DKO (n = 7)
LVmass/BW(mg/g)	4.99 ± 0.30	6.64 ±0.31 *	11.91 ±0.66 $^{*,\#}$	6.25 ± 0.48 *
HR (bpm)	497 ± 16	509 ± 21	471 ± 11	446 ± 25
PWd (mm;	D.93 ± 0.05	0.71 ± 0.03 $^{*,\#}$	1.29 ± 0.07 *	1.18 ± 0.05 *
PWs (mm)	1.43 ± 0.07	0.88 ± 0.04 $^{*,\#}$	1.53 ± 0.06	1.46 ± 0.05
ESD (mm)	2.17 ± 0.04	3.87 ± 0.10 $^{*,\#}$	3.34 ± 0.14 $^{*,\#}$	2.38 ± 0.12
EDD (mm)	3.43 ± 0.09	4.52 ± 0.12 $^{*,\#}$	4.18 ± 0.17 $^{*,\#}$	3.36 ± 0.16
FS (%)	36.62 ± 0.91	14.45 ± 1.67 $^{*,\#}$	20.05 ± 1.16 $^{*,\#}$	29.01 ± 1.91 *
EF (%)	67.40 ± 1.17	30.60 ±3.11 $^{*,\#}$	41.28 ± 2.01 $^{*,\#}$	56.57 ± 2.86 *
	Pressure-volume loop analysis			
	WT (n = 9)	MLP$^{-/-}$ (n = 6)	MYBPC3$^{-/-}$ (n = 6)	DKO (n = 6)
HR (bpm)	394 ± 17	412 ± 29	434 ± 17	408 ± 13
ESP (mmHg)	99.75 ± 3.41	85.07 ± 2.69 *	88.86 ± 5.92	80.39 ±3.08 *
EDP (mmHg)	5.53 ± 0.49	9.70 ± 1.66 *	9.56 ± 1.37 *	10.53 ± 1.98 *
ESV (μL)	15.19 ± 2.00	27.61 ± 1.90 $^{*,\#}$	26.89 ± 1.59 $^{*,\#}$	16.28 ± 1.21
EDV (μL)	24.49 ± 1.41	36.54 ± 1.46 $^{*,\#}$	32.79 ± 1.36 $^{*,\#}$	23.31 ± 1.38
EF(%)	46.57 ± 5.86	31.08 ±3.61 $^{*,\#}$	26.84 ±3.99 $^{*,\#}$	39.58 ±4.19
dP/dt max(mmHg/s)	7174.2 ± 517.8	4496.4 ± 196.8 $^{*,\#}$	8166.3 ± 534.5	7851.0 ± 504.8
t_d (ms)	47.50 ± 3.21	43.30 ± 3.49	25.89 ± 1.55 *	28.10 ± 1.10 *
ET (ms)	53.30 ± 2.62	54.25 ± 2.82 $^{*,\#}$	38.98 ± 1.60 $^{*,\#}$	48.05 ± 2.31
IVRT (ms)	24.55 ± 1.71	34.74 ±2.28 *	33.24 ±2.71 *	33.03 ± 1.42 *
T (ms)	6.90 ± 0.40	10.61 ± 0.49 *	9.87 ± 0.45 *	10.32 ± 0.32 *
S:D	0.71 ± 0.03	0.93 ±0.11 $^{*,\#}$	0.51 ± 0.02 *	0.61 ± 0.02

Echocardiography assessment: BW, body weight; LV Mass/BW, ratio of LV and body weight; HR, heart rate; PWd, posterior wall thickness in diastole; PWs, posterior wall thickness in systole; ESD, end systolic diameter; EDD, end diastolic diameter; FS, fractional shortening; EF, ejection fraction. Pressure-volume loop analysis: HR, heart rate; ESP, end systolic pressure; EDP, end diastolic pressure; ESV, end systolic volume; EDV, end diastolic volume; EF, ejection fraction; dP/dt_{max}, maximum rate of pressure development; td, time to dP/dt_{max}; ET, ejection time; IVRT, isovolumic relaxation time; τ, time constant of pressure relaxation; S:D, systolic to diastolic duration ratio. Values are expressed as mean ± SEM.

*Significantly different from WT (p b 0.05).

#Significantly different from DKO (p b 0.05).